Int. J. Heat Mass Transfer. Vol. 15, pp. 637–653. Pergamon Press 1972. Printed in Great Britain

A DROPLET INTERCHANGE MODEL FOR ANNULAR-DISPERSED, TWO-PHASE FLOW

E. O. MOECK
Atomic Energy of Canada Limited, Chalk River, Canada

and

J. W. STACHIEWICZ
Department of Mechanical Engineering, McGill University, Montreal, Canada

(*Received* 19 *January* 1971 *and in revised form* 27 *June* 1971)

Abstract—An analysis of annular-dispersed flow is presented in which the flow is modelled as a two-dimensional film and a one-dimensional, droplet laden gas core. The focus of the analysis is droplet interchange between core and film and its associated momentum transfer. The intensity of droplet deposition and entrainment governs the axial velocity of each drop size and allows calculation of a maximum stable drop diameter, in good agreement with Wicks' measurements.

An exponential radial void distribution together with a modified universal velocity profile through the film allow calculation of mean and film crest thicknesses from a given film flow rate. These agree well with Harwell data as does the calculated film crest velocity. Interfacial friction factors due solely to profile drag are also calculated and found to agree approximately with Wallis' values for flows with negligible entrainment.

NOMENCLATURE

a, skewness parameter, equation (21) [dimensionless];
A, cross-sectional area of channel, $= \pi R^2$ for a tube [ft^2];
A_c, core cross-section, $= \pi(R - T)^2$ for a tube [ft^2];
B, thickness of liquid base layer, $B^+ = Bu^*\rho_L/\mu_L$ [ft];
c_0, constant, = 0·4, equation (10) [dimensionless];
c_1, constant, = 63·5, equation (10) [dimensionless];
c_D, drag coefficient for a sphere [dimensionless];
c_{WD}, constant, equation (34) [dimensional];
dv, volume fraction of spray of diameter D to $(D + \Delta D)$, in Lagrangian coordinates [dimensionless];
dv', as above but in Eulerian coordinates [dimensionless];
D, droplet diameter; D_{max} = maximum drop diameter [ft];
D^*, $= D/D_{max}$ [dimensionless];
E, transverse entrainment flux, $dE =$ for droplets of diameter D to $(D + \Delta D)$ [lb/ft^{2}s];
f, friction factor, f_i = interface, equation (35) [dimensionless];
F_D, drag force on all droplets per ft^3 of core [lbf/ft^3];
$\mathscr{F}$, drag force on one droplet, equation (8) [lbf];
g, gravitational acceleration, = 32·2 [ft/s^2];
g_0, conversion constant, = 32·2 [lb ft/lbfs^2];
H, distance from wall to film crest $H^+ = Hu^*\rho_L/\mu_L$ [ft];
k, mass transfer coefficient for droplets of size D to $(D + \Delta D)$ [ft/s];
$\bar{k}$, mass transfer coefficient averaged over all drop sizes [ft/s];

k_s, sand roughness height [ft];
M, transverse deposition flux, dM = for droplets of size D to $(D + \Delta D)$ [lb/ft^{2}s];
n, constant, = 0·8, equation (10) [dimensionless];
p, perimeter, = $2\pi R$ for a tube; p_i for the core, = $2\pi(R - T)$ for a tube [ft];
P, pressure [lbf/ft^2 abs];
q_j, coefficients, equation (20) [dimensionless];
r, radius [ft];
R, hydraulic radius, R_{hc} = hydraulic radius of core = $(R - H)$ for a tube [ft];
Re, Reynolds' number, $Re_F = 4W_F/p\mu_L$, Re'_G = superficial gas Re (based on $\bar{u}'_G$ and R) [dimensionless];
T, mean film thickness, $T^+ = Tu^*\rho_L/\mu_L$ [ft];
u, velocity, u_D = of droplets size D to $(D + \Delta D)$ [ft/s];
$\bar{u}$, average velocity based on area occupied by the phase in question [ft/s];
$\bar{u}'_G$, superficial gas velocity, $W_G/(\rho_G A)$ [ft/s];
u^*, friction velocity, $= \sqrt{\tau_w g_0/\rho_L}$ [ft/s];
u^+, $= u/u^*$ [dimensionless];
u_s, $= \sqrt{g_0 dP/d\rho_G}$, the sonic velocity in the core region [ft/s];
U^*, relative velocity [dimensionless];
v, refer to dv;
W, flow rate [lb/s or lb/h];
We_{crit} critical Weber number [dimensionless];
y, coordinate normal to wall $y^+ = yu^*\rho_L/\mu_L$ [ft];
z, axial coordinate [ft].

Greek letters

α, local void fraction, α_c = core average [ft^3 gas/ft^3 of channel];
$\bar{\alpha}$, cross-sectional average void fraction;
β, constant, = 5·5;
δ, size distribution parameter, equation (21) [dimensionless];
Δ, increment;
θ, $= \pi/2$ for upflow;
μ, dynamic viscosity [lb/ft s];
ρ, specific weight [lb/ft^3];
σ, surface tension [lbf/ft];
τ, shear stress [lbf/ft^2];
χ, von Karman constant, = 0·4 [dimensionless].

Subscripts (unless otherwise specified among the main symbols)

c, core;
D, droplets;
F, film;
G, gas;
H, at $y = H$;
i, at film–core interface;
L, liquid;
max, maximum;
T, at $y = T$;
w, at $y = 0$.

INTRODUCTION

THIS PAPER presents a model of the 'annular-dispersed' flow regime, commonly observed in cocurrent gas–liquid systems, and of practical importance in boiling water reactors. Droplet interchange between film and core is the focus of the analysis which leads to equations for droplet slip velocity and a maximum stable drop diameter—neither of which could be predicted from previous theories.

Of the several analyses proposed in the literature the more recent ones include liquid entrainment [1–3, 5, 6] while others, especially the earlier ones, do not. Levy [1] and Wallis [5] proposed annular-dispersed flow models which have a two-dimensional, all-liquid film and a one-dimensional core. They lumped entrained liquid with the gas into a pseudo-fluid travelling at gas velocity. Wallis pointed out [4] that his interfacial friction factor and Levy's dimensionless correlating function are similar. Both are

empirical inputs required to correlate the parameters W_F, T, $(-dP/dz)$ and $\bar{\alpha}$.

Biasi *et al.* [3] introduced

(i) a linear void profile through the film, and

(ii) a two-dimensional gas core.

They calculated the velocity of the entrained liquid at the expense of an additional input for which they chose $\bar{\alpha}$. Since $\bar{\alpha}$ is usually one of the unknowns, requiring it as input detracts from the usefulness of their model. Nishikawa *et al.* [2] described the film and core in much greater detail than any of the other investigators but found that many of the input parameters such as mean roll wave volume and wave velocity are unknown. Pogson *et al.* [6] obtained an empirical correlation of film thickness in terms of dimensionless flow and property parameters and then used single phase diffusivities to obtain a film velocity profile and hence film flow rate. Since they were interested only in film behaviour, they did not specify how to convert calculated T, W_F and τ_w into (dP/dz) and $\bar{\alpha}$.

The relationships between input and output of the various annular-dispersed models (for given

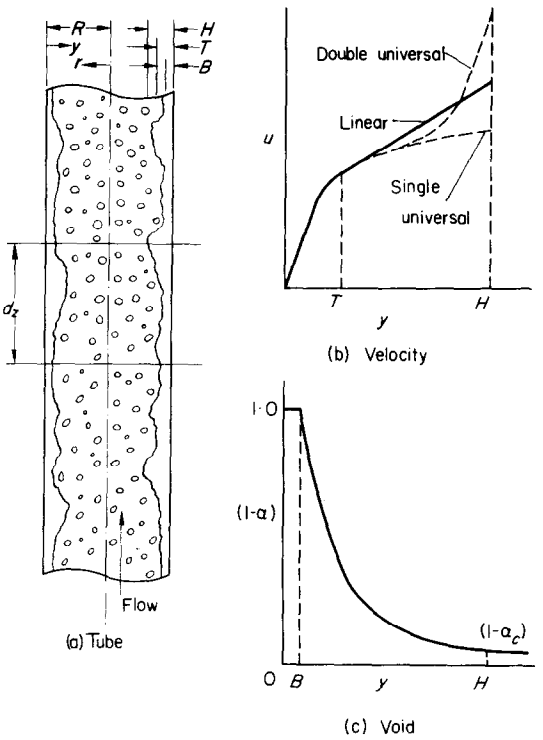

FIG. 1. Annular-dispersed flow model.

Correlation	Input	Output
Levy [1]	$(-dP/dz)$, $\bar{u}_G/\bar{u}_D = 1{\cdot}0$	W_F, T, $\bar{\alpha}$
Wallis [5]	W_F, $\bar{u}_G/\bar{u}_D = 1{\cdot}0$	$(-dP/dz)$, T, $\bar{\alpha}$
Biasi *et al.* [3]	$(-dP/dz)$, $\bar{\alpha}$	W_F, H, $\bar{u}_G/\bar{u}_D \neq 1{\cdot}0$
Nishikawa *et al.* [2]	$(-dP/dz)$, W_D, $\bar{k}$, B, etc.	Base film flow rate, roll wave flow rate, etc.

overall flow rates, fluid properties and tube diameter) are summarized below:

DROPLET INTERCHANGE MODEL

In our model, the flow is divided into a one-dimensional, droplet-laden gas core and a two-dimensional film, as illustrated in Fig. 1(a). In comparison to the above models, ours requires W_F and $\bar{k}$ as input and yields $(-dP/dz)$, $\bar{\alpha}$, $\bar{u}_G$, $\bar{u}_D$, T, H, D_{max} etc. as output.

Film analysis

To relate film thickness, film flow rate and interface velocity, void and velocity profiles through the film are required. We made three main assumptions and supported them with experimental evidence where possible.

(1) A continuous liquid base layer of thickness B, in contact with the wall, supports an intermittent layer of thickness $(H-B)$.

Figure 2(a) shows measured base layer thicknesses of five investigators [2, 7–10]. They observed that gas velocity and not liquid flow rate has the dominant influence on B. Their results cluster in a band which can be empirically correlated by

$$\frac{B}{R} = 1{\cdot}05 \times 10^4 Re'_G{}^{-5/4}. \quad (1)$$

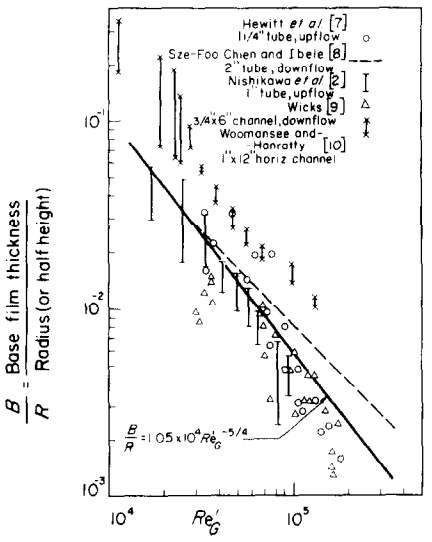

(a) Base film thickness in air–water flow

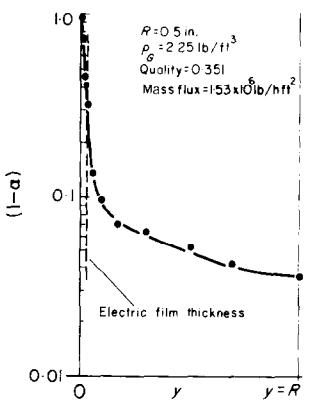

(b) Void profile in argon–water flow [11]

FIG. 2. Base film thickness and void profile data.

The data of Hanratty and Woodmansee [10] fall above this band probably because the peak in their velocity profile was distorted towards the smooth ceiling wall of the duct so that the characteristic length is greater than the channel half-height R.

(2) The local void fraction is zero in the base layer but increases exponentially to core void fraction at $y = H$, as illustrated in Fig. 1(c).

Hewitt *et al.* [7] and others observed that the needle probe indicated less frequent contact with liquid as y increased. This fact is approximated by

$$\alpha = 0 \qquad \text{for } 0 \leq y \leq B$$

$$(1 - \alpha) = (1 - \alpha_c)^{\frac{y-B}{H-B}} \qquad \text{for } B < y \leq H. \quad (2)$$

(When all liquid is in the film, $\alpha_c = 0$. To obtain a finite profile, an arbitrary limit is imposed by specifying $\alpha_c \leq 0{\cdot}9999$.) Figure 2(b) shows data of Adorni *et al.* [11] who observed that $(1 - \alpha)$ drops exponentially near the wall and is nearly independent of radius in the core, as assumed in our model.

(3) The liquid velocity in the film follows the 'universal profile' from the wall to mean thickness T. From T to H, the profile is linear, as illustrated in Fig. 1(b). Wall curvature is neglected.

Since there are no measurements applicable to annular-dispersed flow, all previous investigators assumed either a velocity profile, diffusivity or friction factor based on single phase flows. The present assumption is a compromise between 'double' and 'single' universal profiles, first suggested by Anderson and Mantzouranis [12]. We agree with their suggestion that the real profile lies between these two because the free liquid surface is not damped to the same extent as one in contact with a solid boundary. There are no direct data which could be used to support this hypothesis, but McPherson's measurements [13] show conclusively that, in horizontal shear flow without entrainment, the single universal profile underestimates film velocities.

We chose Spalding's expression [14] for the universal profile in the region $0 \leq y^+ \leq T^+$ because it is continuous in y^+,

$$y^+ = u^+ + \exp(-\chi\beta)\left[\exp(\chi u^+) - 1 - \chi u^+ - \frac{(\chi u^+)^2}{2} - \frac{(\chi u^+)^3}{3}\right]. \quad (3)$$

At large y^+,

$$u^+ \simeq \frac{1}{\chi} \ln y^+ + \beta,$$

therefore $\chi = 0{\cdot}4$ and $\beta = 5{\cdot}5$ to agree with von Karman's turbulent profile. The validity of this representation is discussed at the end of this paper.

At $y^+ = T^+$, the velocity and velocity gradient were matched to a linear profile, so that for $T^+ < y^+ \leq H^+$,

$$u^+ = u_T^+ + (y^+ - T^+)\left[\frac{\mathrm{d}u^+}{\mathrm{d}y^+}_{y^+ = T^+}\right]. \quad (4)$$

The flow rate in the disturbed film can now be obtained by integration,

$$\frac{W_F}{p\mu_L} = \int_0^{B^+} u^+ \mathrm{d}y^+ + \int_{B^+}^{T^+} (1 - \alpha) u^+ \mathrm{d}y^+ + \int_{T^+}^{H^+} (1 - \alpha) u^+ \mathrm{d}y^+. \quad (5)$$

The first and third integrals can be evaluated analytically, but a numerical integration is required for the second.

Finally, we defined a mean film thickness T^+ such that an all-liquid, smooth film having a universal velocity profile has the same flow rate as the disturbed film,

$$\frac{W_F}{p\mu_L} = \int_0^{T^+} u^+ \mathrm{d}y^+ \quad (6)$$

where u^+ and y^+ are related by equation (3).

Equations (1–6) provide sufficient relations to solve for B^+, T^+, H^+ and their corresponding velocities, by iteration, for given W_F, Re_G, τ_w and α_c. The next section provides relations for α_c and other parameters.

Core analysis

Photographic and other studies, performed at several laboratories, indicate that there is continual interchange of liquid, by deposition and entrainment, between the fast-moving core and the slow-moving film. Therefore, in a fully developed flow, the entrained liquid must—on the average—travel slower than the gas and thus be always in a state of acceleration. This concept departs from previous analyses and provides equations relating drop size and drop velocity to known parameters.

We assumed that the entrained liquid is a cloud of spherical droplets of various size, travelling at different axial velocities, depending on their size, in an infinite, one-dimensional, turbulent gas stream. The number of droplets per unit core volume, $\mathrm{d}N$, of diameter D to $(D + \Delta D)$ is given by

$$\mathrm{d}N = \frac{6(1 - \alpha_c)}{\pi D^3} \mathrm{d}v \quad (7)$$

and the drag force on $\mathrm{d}N$ is

$$\mathrm{d}F_D = \mathscr{F} \mathrm{d}N$$

where

$$\mathscr{F} = \frac{1}{2}\left(\frac{\pi D^2}{4}\right) c_D \frac{\rho_G}{g_0} (\bar{u}_G - u_D)^2. \quad (8)$$

The drag force per unit core volume is then

$$F_D = \tfrac{3}{4}(1 - \alpha_c) \frac{\rho_G}{g_0} \int_0^1 \frac{c_D (\bar{u}_G - u_D)^2}{D} \mathrm{d}v. \quad (9)$$

Karnis *et al.* [14] reviewed the literature on drag coefficients for accelerating particles and found that c_D values obtained by some researchers fell below the steady state curve while those obtained by others fell above. Therefore, we chose the steady state drag coefficient and approximated it by the relation

$$c_D = c_0(1 + c_1 Re_D^{-n}) \quad (10)$$

where

$$Re_D = \rho_G(\bar{u}_G - u_D)/\mu_G$$

and for $0{\cdot}5 < Re_D < 10^5$, approximate values of the constants are

$$c_0 = 0{\cdot}4, \quad c_1 = 63{\cdot}5, \quad n = 0{\cdot}8.$$

Another relation for F_D can be obtained from a momentum balance on the droplet cloud in fully developed flow. The forces under consideration are:

Buoyancy

$$= -\frac{g}{g_0}\left[\int_0^1 (1-\alpha_c)(\rho_L-\rho_G)\mathrm{d}v\right]A_c\mathrm{d}z\sin\theta$$

Gas drag $= F_D A_c \mathrm{d}z$

$$\text{Entrainment} = \left[\int_0^E u_H \mathrm{d}E\right]p_i\mathrm{d}z/g_0$$

$$\text{Deposition} = -\left[\int_0^M u_D \mathrm{d}M\right]p_i\mathrm{d}z/g_0$$

By definition, $E = M$, hence

$$F_D = \frac{g}{g_0}(1-\alpha_c)(\rho_L-\rho_G)\sin\theta\int_0^1 \mathrm{d}v + \frac{2}{g_0 R_{hc}}\int_0^M (u_D-u_H)\mathrm{d}M. \quad (11)$$

To continue with the analysis, we assumed that the size spectrum of droplets leaving the film by entrainment and entering the film by deposition is identical to that of the droplets in the core. Under this assumption, the deposition flux of droplets of size D to $(D + \Delta D)$ is

$$\mathrm{d}M = \rho_L(1-\alpha_c)k\mathrm{d}v. \quad (12)$$

The mass transfer coefficient k is not normally known, but an average $\bar{k}$ over all drop sizes has been measured by, for example, Cousins and Hewitt [16]. They defined

$$M = \bar{k}\rho_G W_D/W_G \quad (13)$$

from which

$$\mathrm{d}M = \frac{\bar{k}\rho_G}{W_G}\mathrm{d}W_D. \quad (14)$$

Now, the continuity equations for the droplets and the gas are

$$\mathrm{d}W_D = \rho_L u_D(1-\alpha_c)A_c\mathrm{d}v$$

$$W_G = \rho_G \bar{u}_G \bar{\alpha} A$$

so that

$$k = \left(\bar{k}\frac{u_D}{\bar{u}_G}\right)\left(\frac{A_c}{\bar{\alpha}A}\right). \quad (15)$$

In annular-dispersed flow, the factor $(A_c/\bar{\alpha}A)$ is very close to unity since the area available for gas flow, $\bar{\alpha}A$, is about the same as the area of the core, A_c. Consequently,

$$k \simeq \bar{k}\frac{u_D}{\bar{u}_G}. \quad (16)$$

Equation (11) can now be rewritten as

$$F_D = \frac{g}{g_0}\rho_L(1-\alpha_c)\int_0^1\left[\left(1-\frac{\rho_G}{\rho_L}\right)\sin\theta + \left(\frac{2\bar{k}u_D}{gR_{hc}\bar{u}_G}\right)(u_D-u_H)\right]\mathrm{d}v. \quad (17)$$

When equations (9) and (17) are equated and differentiated with respect to $\mathrm{d}v$, the following relation between droplet diameter D and velocity u_D is obtained,

$$\left(\frac{3R_{hc}\rho_G\bar{u}_G}{8\rho_L\bar{k}}\right)\frac{c_D}{D}\left(1-\frac{u_D}{\bar{u}_G}\right)^2 = \left(\frac{gR_{hc}\sin\theta}{2\bar{k}\bar{u}_G}\right)\left(1-\frac{\rho_G}{\rho_L}\right) + \frac{u_D}{\bar{u}_G}\left(\frac{u_D}{\bar{u}_G}-\frac{u_H}{\bar{u}_G}\right). \quad (18)$$

The slip velocity $(\bar{u}_G - u_D)$, implied in this equation, increases with drop diameter, so that the dynamic gas pressure on the large droplets can become sufficiently large to overcome the restoring surface tension force and cause droplet breakup. The relation between these opposing forces is given by a critical Weber number,

$$We_{\mathrm{crit}} = \frac{D_{\max}\rho_G(\bar{u}_G-u_D)^2}{\sigma g_0} \quad (19)$$

where We_{crit} has the classical value of 13 or 22 [17].

The maximum stable drop diameter, $D_{\max}$, and its velocity $u_{D_{\max}}$ can now be obtained from equations (18) and (19). In terms of velocity, this gives

$$q_3 U_{\max}^{*4+n} + q_2 q_5^n U_{\max}^{*4} - q_5^{1+n}[U_{\max}^{*2} - q_1 U_{\max}^{*} + q_4] = 0 \quad (20)$$

where

$$U^*_{\max} = \left(1 - \frac{u_{D_{\max}}}{\bar{u}_G}\right); \quad q_1 = \left(2 - \frac{u_H}{\bar{u}_G}\right)$$

$$q_2 = \frac{3R_{hc}\rho_L c_0 \bar{u}_G}{8\rho_L \bar{k}}; \quad q_3 = q_2 c_1 \left(\frac{\mu_G}{\rho_G \bar{u}_G}\right)^n$$

$$q_4 = \frac{R_{hc} g \sin\theta}{2\bar{k}\bar{u}_G}\left(1 - \frac{\rho_G}{\rho_L}\right) + \left(1 - \frac{u_H}{\bar{u}_G}\right);$$

$$q_5 = \frac{\sigma g_0 We_{\text{crit}}}{\rho_G \bar{u}_G^2}$$

and the root of interest is in the range

$$0 < U^*_{\max} < \left(1 - \frac{u_H}{\bar{u}_G}\right).$$

To test the core analysis, we require measurements of $D_{\max}$ (or $u_{D_{\max}}$), $\bar{k}$ and u_H in addition to the normally recorded flow rates and fluid properties. The film crest velocity u_H is expected to be a minor factor, so that principally $D_{\max}$ and $\bar{k}$ are required. We know of no simultaneous measurements of these in fully developed annular-dispersed flow. Wicks [9] obtained the most detailed drop size spectra, while Cousins and Hewitt [16] measured $\bar{k}$ and obtained approximate drop size distributions. Fortunately, they found that $\bar{k}$ was independent of air velocity, tube diameter and air pressure. Therefore, we made the key assumption that their $\bar{k}$ also applies to Wicks' experiments and solved equation (20) for Wicks' conditions:

R_{hc} = 1/16 ft (zero film thickness)
ρ_G = 0·0750, ρ_L = 62·4 lb/ft^3
μ_G = 1·212 × 10^{-5} lb/fts
σ = 4·94 × 10^{-3} lbf/ft
u_H = 0·07 $\bar{u}_G$ (assumed)
$\bar{k}$ = 0·8 ft/s (assumed)
We_{crit} = 13 (assumed).

Figure 3 compares experimental and calculated maximum drop diameters. The data are correlated very well by the reference curve except at the highest water flow rates of 4000 and 5200 lb/h. Wicks noted that liquid bridging probably contributed to erroneously large apparent drop sizes at those liquid rates.

To test the influence of the assumed values of We_{crit}, $\bar{k}$ etc. on the solution, each parameter was perturbed in turn and $D_{\max}$ calculated. The results are shown in Fig. 3 and are further discussed in the section "Discussion of Main Assumptions".

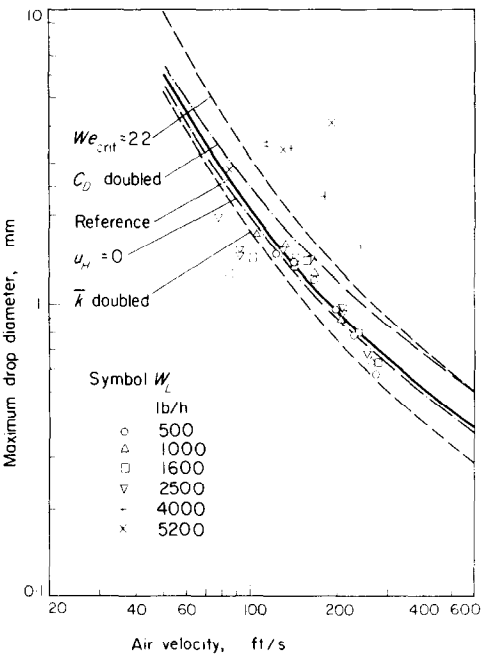

FIG. 3. Theoretical maximum drop size, reference curve equation (20), compared with data of Wicks [9].

To calculate the droplet drag force F_D per unit core volume a drop size spectrum is required. The one adopted in this study was proposed by Mugele and Evans [18]. It is called the 'upper-limit log normal distribution' and is of the form:

$$\frac{dv'}{dD} = \frac{D_{\max}\delta}{D(D_{\max} - D)\sqrt{\pi}} \exp - \left[\delta \ln\left(\frac{aD}{D_{\max} - D}\right)\right]^2. \quad (21)$$

Equation (21) is one of the many spectral distributions that could be used, but it is the only one which takes into account the presence of a maximum drop size. Its validity for annular two-phase flow was conclusively demonstrated in an exhaustive study of Wicks [9] who was able to correlate very well his experimental measurements of drop-size spectra by means of equation (21). From his measurements the following values of a and δ can be obtained:

$$a = 4{\cdot}0, \quad \delta = 0{\cdot}738.$$

We assumed that these are applicable to other flow conditions, and used them in our model.

Although it could be argued that the numerical constants may not be universal, no reliable results are at present available to suggest other values, and if such results do become available in the future, they can easily be incorporated into our model.

where

$$\bar{u}_D = \int_0^1 u_D \, dv. \tag{23}$$

This conversion can be done numerically. Figure 4 illustrates one set of calculations for air–water upflow, run 509 of Gill *et al.* [19], for which

dia. = 1·25 in.	$\lvert dP/dz \rvert$ = 28·77 lbf/ft^3
W_G = 500 lb/h	ρ_G = 0·1141 lb/ft^3
W_L = 1000 lb/h	$\bar{k}$ = 0·8 ft/s (assumed)
W_F = 428 lb/h	D_{max} = 1034 μ (calculated)

Momentum and continuity equations

The formulations presented up to this point could be incorporated into the continuity and momentum equations for fully developed, incompressible, adiabatic flow. This would represent the simplest case. However, a search of the literature did not reveal any suitable data with which to compare predictions. Therefore slowly developing, compressible, adiabatic upflow in a round tube will now be modelled and compared with three sets of data.

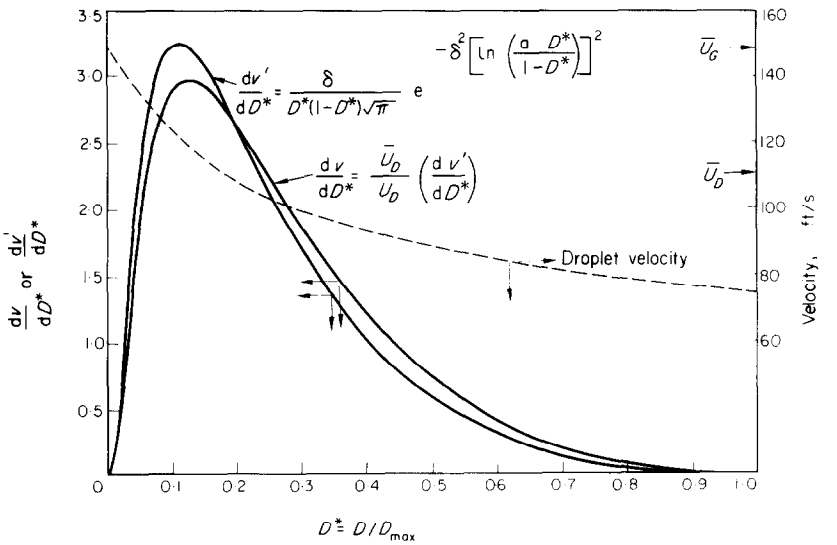

FIG. 4. Calculated drop size spectra and drop velocity for Run 509 of Gill *et al.* [19].

Before this spectrum can be applied to the present analysis, it must be converted from Eulerian coordinates dv' to Lagrangian coordinates dv, according to the relation

$$dv' = u_D \, dv/\bar{u}_D \tag{22}$$

The following forces are considered:

(a) For the entire cross section

$$\text{Gravity} = -\frac{g}{g_0}\pi R^2\,\mathrm{d}z[\rho_G + (1-\bar{\alpha})(\rho_L-\rho_G)]$$

$$\text{Wall shear} = -2\pi R\tau_w\,\mathrm{d}z$$

$$\text{Pressure} = -\pi R^2\,\mathrm{d}P$$

$$\text{Acceleration} = -\frac{1}{g_0}\mathrm{d}[W_G\bar{u}_G + W_D\bar{u}_D + W_F\bar{u}_F]$$

$$\left(-\frac{\mathrm{d}P}{\mathrm{d}z}\right) = \frac{2\tau_w}{R} + \frac{g}{g_0}\rho_L\left[1-\bar{\alpha}\left(1-\frac{\rho_G}{\rho_L}\right)\right] + \frac{1}{g_0\pi R^2}\frac{\mathrm{d}}{\mathrm{d}z}[W_G\bar{u}_G + W_D\bar{u}_D + W_F\bar{u}_F]. \quad (24)$$

(b) For the gas core

$$\text{Gravity} = -\frac{g}{g_0}\pi R^2\rho_G\,\mathrm{d}z$$

$$\text{Interfacial shear} = -2\pi(R-T)\tau_i\,\mathrm{d}z$$

$$\text{Pressure} = -\pi(R-T)^2\,\mathrm{d}P$$

$$\text{Droplet drag} = -F_D\pi(R-T)^2\,\mathrm{d}z$$

$$\text{Acceleration} = -\frac{W_G}{g_0}\mathrm{d}\bar{u}_G$$

$$\left(-\frac{\mathrm{d}P}{\mathrm{d}z}\right) = \frac{g}{g_0}\rho_G\left(\frac{R}{R-T}\right)^2 + F_D + \frac{2\tau_i}{(R-T)} + \frac{W_G}{\pi(R-T)^2 g_0}\frac{\mathrm{d}\bar{u}_G}{\mathrm{d}z}. \quad (25)$$

(c) For the droplet cloud

Terms given in equation (11) plus

$$\text{Acceleration} = -\frac{1}{g_0}\mathrm{d}(W_D\bar{u}_D)$$

$$F_D = \frac{g}{g_0}(1-\alpha_c)(\rho_L-\rho_G) + \frac{2}{g_0(R-T)}\left[\int_0^M u_D\,\mathrm{d}M - \int_0^E u_H\,\mathrm{d}E\right] + \frac{1}{g_0\pi(R-T)^2}\frac{\mathrm{d}(W_D\bar{u}_D)}{\mathrm{d}z}. \quad (26)$$

(d) For the liquid film, the momentum balance is implicit in the three equations just presented.

The continuity equations are:

$$W_G = \text{constant}, \quad W_L = W_F + W_D = \text{constant}. \quad (27)$$

Therefore

$$\bar{u}_G = \frac{W_G}{\rho_G\bar{\alpha}\pi R^2} \quad (28)$$

$$\bar{u}_D = \frac{W_D}{\rho_L(1-\alpha_c)\pi(R-T)^2} \quad (29)$$

$$\frac{\mathrm{d}W_D}{\mathrm{d}z} = -\frac{\mathrm{d}W_F}{\mathrm{d}z} = 2\pi(R-T)(E-M). \quad (30)$$

The average void fraction is obtained by integration of the assumed void profile across the tube,

$$\pi R^2\bar{\alpha} = \pi(R-H)^2\alpha_c + \int_{(R-H)}^{(R-B)} 2\pi r\alpha\,\mathrm{d}r$$

which for α_c close to unity gives

$$\bar{\alpha} \simeq \alpha_c\left(1-\frac{H}{R}\right)^2 + (H-B)(2R-H-B)/R^2 + 2\alpha_c\left[\frac{H-B}{R\ln(1-\alpha_c)}\right]^2\left[1+\left(\frac{R-B}{H-B}\right)\ln(1-\alpha_c)\right]. \quad (31)$$

In slowly accelerating flows, the d/dz terms (except pressure gradient) usually do not add more than a few percent to the largest terms. Furthermore, velocities $\bar{u}_D$ and $\bar{u}_F$ are expected to remain very nearly constant with z, because of compensating factors, so that only $\mathrm{d}W_D/\mathrm{d}z$ and $\mathrm{d}\bar{u}_G/\mathrm{d}z$ are retained from here on. Hence equation (24) simplifies to

$$\left(-\frac{\mathrm{d}P}{\mathrm{d}z}\right) = \frac{2\tau_w}{R} + \frac{g}{g_0}\rho_L\left[1-\bar{\alpha}\left(1-\frac{\rho_G}{\rho_L}\right)\right] + \frac{W_G}{g_0\pi R^2}\frac{\mathrm{d}\bar{u}_G}{\mathrm{d}z} + \frac{(\bar{u}_D-u_H/2)}{g_0\pi R^2}\frac{\mathrm{d}W_D}{\mathrm{d}z} \quad (32)$$

where, for simplicity, $\bar{u}_F$ was set equal to $u_H/2$.

The $d\bar{u}_G/dz$ term was evaluated as follows: For a perfect gas

$$\frac{d\bar{u}_G}{dz} = \frac{g_0 \bar{u}_G}{\rho_G u_s^2}\left(-\frac{dP}{dz}\right) \tag{33}$$

while dW_D/dz was correlated empirically. We obtained the following equations from data for air–water upflow in tubes of 3/8 in. dia. [20], 1/2 in. dia. [21] and 1·25 in. dia. [22],

$$\frac{d(W_D/W_L)}{d(z/R)} = c_{WD}\bar{u}_G^2 Re_F^{-1/4}\left[-\frac{dP}{d(z/R)}\right] \tag{34}$$

where $c_{WD} = 2{\cdot}79 \times 10^{-8}$, $5{\cdot}44 \times 10^{-8}$ and $11{\cdot}27 \times 10^{-8}$ s^2/lbf for the three tubes, respectively. Figure 5 compares the experimental

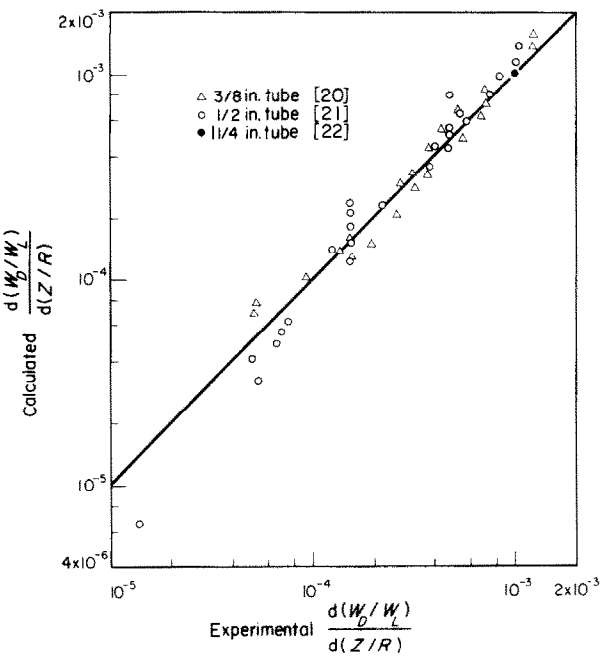

FIG. 5. Empirical correlation of net entrainment rate.

entrainment gradient with values calculated from equation (34). The right hand side of that equation was evaluated at an axial location far from the inlet (where pressure and entrainment gradients are constant), namely at 96, 107 and 209 in. for the three tubes, respectively.

This completes the system of equations. They were solved numerically, by iteration [23], as follows: For given pipe radius, fluid properties, W_G, W_L, W_F, $(-dP/dz)$ and $\bar{k}$, the average film thickness T and crest velocity u_H were calculated from the film analysis. Average drop velocity $\bar{u}_D$ was obtained from the core analysis, and drag force F_D from equation (26). Void fractions α_c and $\bar{\alpha}$ were also obtained. Iteration on α_c and T proceeded until τ_w from u^*, used in the film analysis, matched τ_w from equation (32). At this point T, u_H, $\bar{u}_D$, α_c, $\bar{\alpha}$, F_D, τ_i, etc. converged to satisfy the momentum and continuity equations.

Analogously to single phase flow, we defined an interfacial friction factor from the shear stress τ_i,

$$f_i = \frac{\tau_i}{\frac{1}{2}\frac{\rho_G}{g_0}(\bar{u}_G - u_H)^2} \tag{35}$$

which was also an output of the calculations.

COMPARISON WITH AIR–WATER DATA

We selected three sets of air–water data from the literature and used these as input to the computer program. The data are for upflow in tubes of

(i) 3/8 *in. dia.* Cousins *et al.* [20], AERE-R4926. 21 tests at $W_L \geq 75$ lb/h were selected since at lower liquid flows the entrained fraction was negligible.

(ii) 1/2 *in. dia.* Hinkle [21]. All 27 runs were processed.

(iii) 1·25 *in. dia.* Gill *et al.* [19], AERE-R3955. 41 tests, for which the frictional pressure drop was larger than the gravitational head, were selected.

These were chosen because

sufficient variables were measured to obtain W_F and $(-dP/dz)$ in addition to W_G and W_L,

the mass transfer coefficient $\bar{k}$ could be estimated from subsequent Harwell studies,

the net entrainment gradient could be estimated from equation (34).

All runs were processed with a constant $\bar{k} =$ 0·8 ft/s, based on the measurements of Cousins

and Hewitt [16]. Application of this $\bar{k}$ to Hinkle's data was considered reasonable in view of the similar experimental conditions in those two studies.

Figure 6 shows that the calculated mean film thickness T agrees well with experimental values for the 1·25 in. dia. tube. No film thicknesses were recorded in the other experiments.

The curves in Fig. 7 are calculated values of H/T for the 1·25 in. tube. This ratio was not

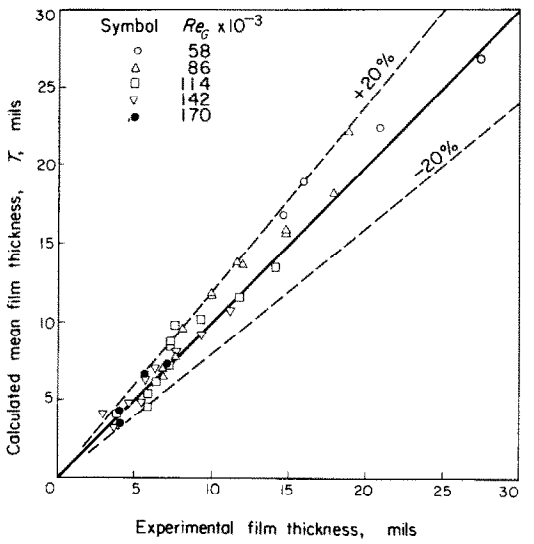

FIG. 6. Mean film thickness in the 1·25 in. dia. tube of Gill *et al.* [19].

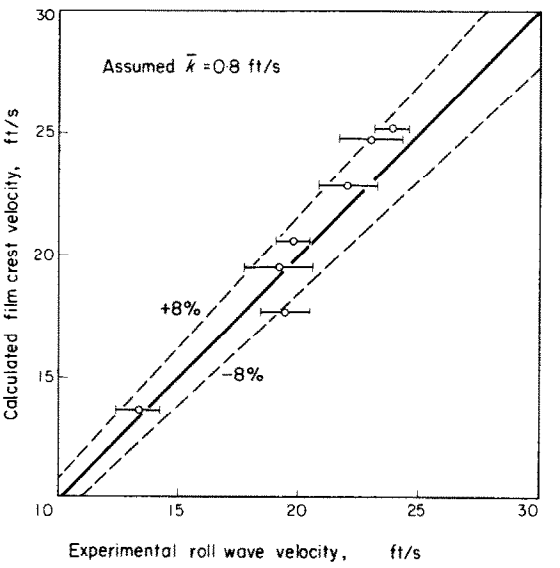

FIG. 8. Film crest velocity in the 1/2 in. dia. tube of Hinkle [21].

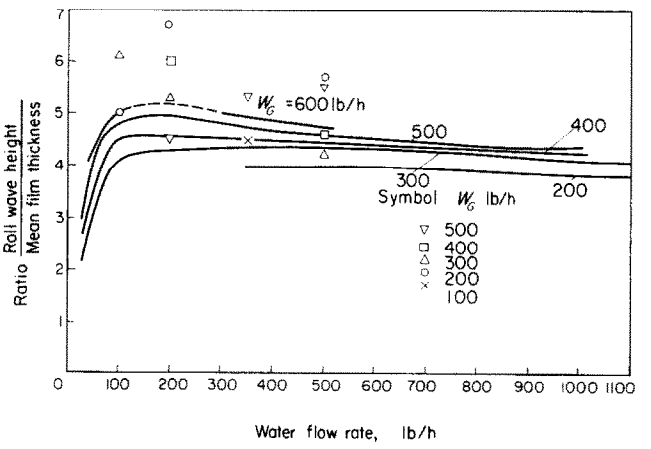

FIG. 7. Calculated film crest-to-mean thickness ratio in a 1·25 in. dia. tube compared with data of Hewitt and Nicholls [24].

reported in [19], but in a later study, Hewitt and Nicholls [24] obtained the average roll wave amplitude as well as mean film thickness under similar, but not identical, conditions. The theory is in acceptable agreement with measurements.

Calculated film crest velocities are compared with measured roll wave velocities in Figs. 8 and 9. Hinkle's data are predicted to within about ± 8 per cent, Fig. 8. Gill *et al.* did not measure roll wave velocities, but, they are reported in subsequent Harwell studies [24], [25] and in a paper by Nedderman and Shearer [26]. Figure 9 shows acceptable agreement between calculated curves and data obtained at similar, but not identical, conditions. The deviations shown are to be expected since both roll wave and film crest velocities are sensitive to W_F, ρ_G, $\bar{u}_G$ which are not necessarily the same for given W_L and W_G.

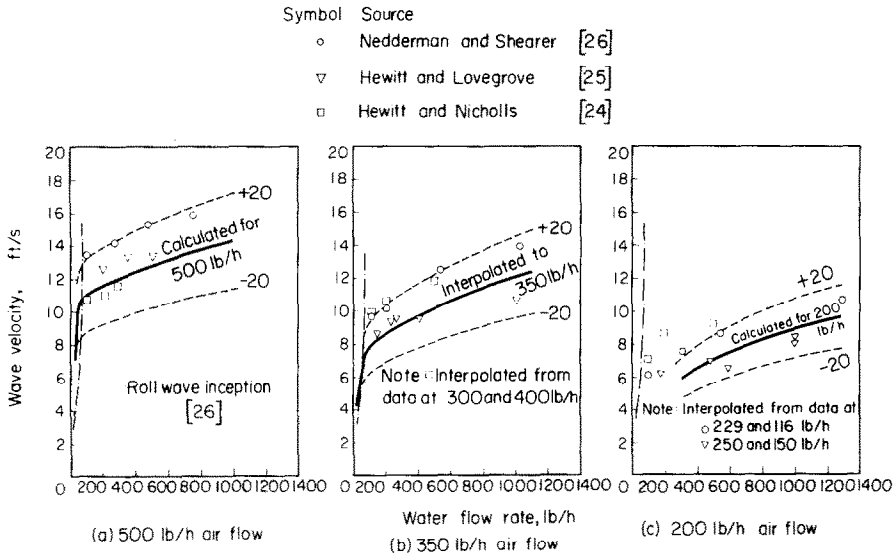

FIG. 9. Calculated and experimental film crest velocities in a 1·25 in. dia. tube.

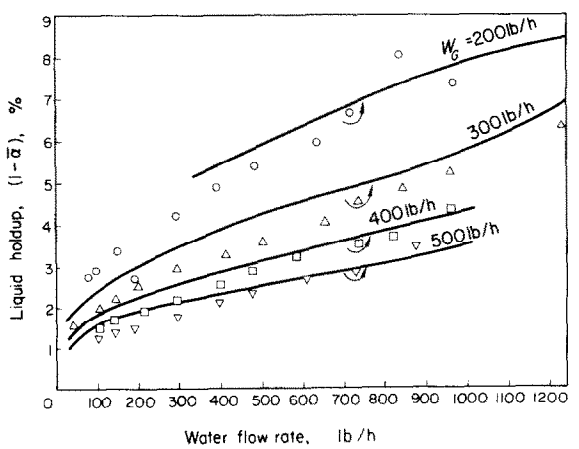

FIG. 10. Calculated liquid holdup in a 1·25 in. dia. tube compared with data of Hewitt *et al.* [27].

Channel-average liquid fractions $(1 - \bar{\alpha})$, calculated for the conditions of Gill *et al.*, are compared with measured liquid holdup data of Hewitt *et al.* [27] in Fig. 10. The predictions are acceptable considering that other system variables such as pressure, pressure drop, and film flow rate were not identical in these two series of experiments.

Interfacial friction factor

As mentioned, interfacial friction factors f_i were calculated from equation (35). Since droplet

drag, static head, acceleration and interface velocity are accounted for in the calculation of τ_i, the friction factor is the best available estimate of wave form drag and viscous friction at the film-core interface. Figure 11 is a plot of f_i against relative film thickness T/R. The data cluster into a single band regardless of

gas Reynolds' number
tube diameter
total liquid flow rate.

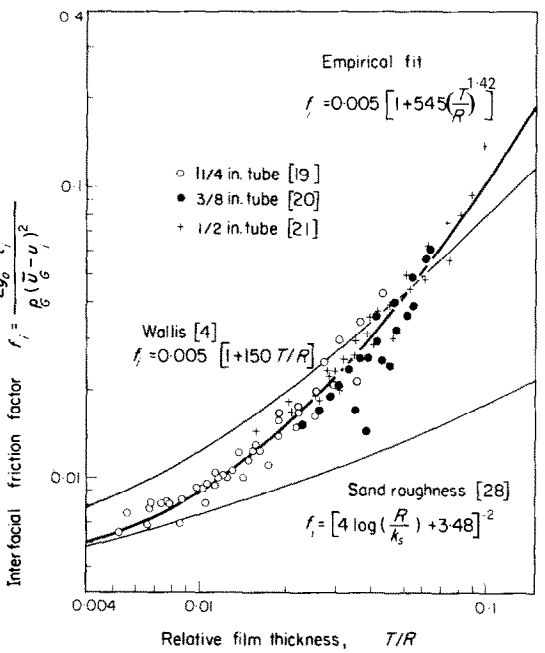

FIG. 11. Empirical correlation of friction factor data.

The third item must be qualified for runs at high entrainment levels (large W_G and W_L), especially for the 3/8 in. dia. tube. At these conditions f_i appears to remain constant or even to decrease with increasing T/R. The most probable reason for this is that the assumed $\bar{k} = 0{\cdot}8$ ft/s is too large for droplet concentrations more than double those studied in [23]. A smaller $\bar{k}$, due to mutual droplet interference and gas turbulence damping, would reduce drag F_D and hence raise f_i back into the cluster.

The friction factor f_i is higher than for sand roughness in the fully turbulent region [28] if one takes $k_s = T$, but agrees approximately with Wallis' friction factors, calculated from flows with negligible entrainment and negligible film interface velocity. f_i can be correlated by the empirical relation

$$f_i = 0{\cdot}005[1 + 545(T/R)^{1{\cdot}42}]. \qquad (36)$$

Other combinations of f_i and relative roughness, such as f_i minus smooth pipe friction factor as a function of $(T - B)/R$, did not improve the correlation.

Equation (36) can be regarded as an alternative to the empirical correlations of Wallis [5] and Levy [1] and therefore introduced into the droplet interchange model to calculate $(-\mathrm{d}P/\mathrm{d}z)$, T, $\bar{\alpha}$, $D_{\max}$, etc. from given

$$W_G,\ W_L,\ W_F,\ \bar{k},\ R \text{ and properties.}$$

Figure 12 illustrates a set of such calculations for run 309 of Gill *et al.* [19]. We assumed a fixed

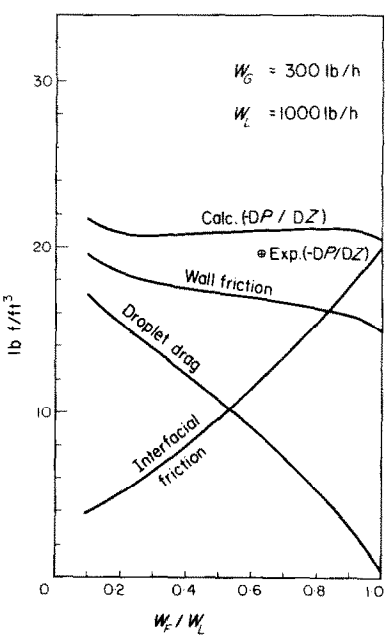

FIG. 12. Calculated forces for Run 309 of Gill *et al.* [19] in a 1·25 in. dia. tube.

$\bar{k} = 0{\cdot}8$ ft/s and allowed W_F to vary from 10 per cent to 100 per cent of W_L. The curves shown are the

droplet drag	F_D from equation (26)
interfacial friction	$2\tau_i/(R - T)$ from equations (35) and (36)
wall friction	$2\tau_w/R$ from equation (32)
pressure gradient	$(-\mathrm{d}P/\mathrm{d}z)$ from equation (25).

The single point is the experimental pressure gradient at the measured W_F/W_L.

Interfacial friction and droplet drag behave as expected: as one increases the other declines. However, $(-\mathrm{d}P/\mathrm{d}z)$, which is very nearly the sum of these two forces, is insensitive to the liquid partition between film and droplets. This implies that an attempt to predict W_F from given $(-\mathrm{d}P/\mathrm{d}z)$ could result in multiple solutions or no solution at all. Since Levy [1] used such a region $B \leq y \leq T$, where voids are present, density and viscosity become functions of y, and hence the use of ρ_L and μ_L (ρ_w and μ_w) in defining u^+ and y^+ represents an idealisation. The other alternative would be to use $\rho(y)$ and $\mu(y)$ in the region $B \leq y \leq T$. Our decision to use ρ_L and μ_L is vindicated by the work of Bankston and McEligot [29], who studied heat transfer to gases with large temperature differences, where density and viscosity varied by factors of up to four within the turbulent boundary layer. They compared various eddy diffusivity models against experimental results and found that better agreement was obtained with models that used wall rather than local properties in non-dimensionalising the variables.

In the region $T \leq y \leq H$, the use of ρ_L and μ_L is even more appropriate, for it means that both the actual and the non-dimensional velocity profiles are linear, which would not be the case if $\rho(y)$ and $\mu(y)$ were used in the non-dimensionalisation.

Parameter	We_{crit}	$\bar{k}$	u_H	R_{hc}^*	c_D
Reference value	13	0·8	$0{\cdot}07\bar{u}_G$	0·0625	c_D
Perturbed value	22	1·6	0	0·0592	$2\,c_D$
Per cent change in parameter	+69	+100	−100	−5·3	+100
Per cent change in D_{max}	+44	−18·3	−5·0	−1·7	+23·8

* Perturbation in R_{hc} corresponds to a 0·020 in. thick film on both plates.

correlating scheme, the divergence between his and the present analysis remains unresolved. Data are required to elucidate the dependence of $(-\mathrm{d}P/\mathrm{d}z)$ on W_F/W_L at constant R, W_G, fluid properties and negligible bulk flow acceleration.

DISCUSSION OF MAIN ASSUMPTIONS

The variables in equation (3) are defined by using the friction velocity and the viscosity of the liquid film at the wall, as is usually done in single phase flow. In the all-liquid base layer ($0 \leq y \leq B$), this procedure is quite appropriate, but in the

The other arbitrary assumptions that were made concerned the constant values of u_H, $\bar{k}$ and We_{crit}, used in calculating the maximum droplet diameter D_{max}. As mentioned already, the influence of these values on the solution was tested by perturbing each parameter in turn, when calculating D_{max}. The results are shown in Fig. 3 and are further illustrated in the following calculations, done for an air velocity of 150 ft/s:

As the above table and Fig. 3 show, the influence of u_H and $\bar{k}$ is relatively secondary, complete omission of u_H causing only a small error. In the subsequent analysis which combines

the film and core models, however, u_H is retained since it is one of the calculated variables. The value of $\bar{k} = 0{\cdot}8$ was based on the work of Cousins and Hewitt [16] (who obtained values of 0·5–1·0 from a large number of tests at varying concentrations, gas and liquid flows and deposition lengths), has also a relatively small effect on results, as a 100 per cent increase in $\bar{k}$ produces only an 18 per cent change in D_{max}.

D_{max} is more sensitive to changes in We_{crit} and here we were faced with the choice of two values appearing in literature: 13 and 22. According to Hinze [17], if the viscosity of the droplet fluid is low, disintegration occurs at $We_{crit} = 13$. For more viscous drops disintegration is delayed and the value of 22 is more suitable. In view of the above a value of 13 was chosen, and Fig. 3 shows that it indeed yields a much better correlation than 22.

DISCUSSION

The droplet interchange model requires $\bar{k}$ as an input. Our search of literature did not reveal a convincing correlation for it and therefore we used the experimental value of $\bar{k} = 0{\cdot}8$ ft/s. Of course the model could just as readily accommodate a variable $\bar{k}$ (or k) based on Reynolds' analogy, that is, $k \propto \sqrt{f_i}$. Whether such a relation is more appropriate will have to be resolved by experiment. Since the droplet cloud is not a continuum and droplet diffusivities are known to be much less than the gas diffusivity, Reynolds' analogy need not necessarily be valid.

The calculated wall friction $2\tau_w/R$ in Fig. 12 did not pass through a minimum, as we expected. In adiabatic single phase flow, irreversible energy dissipation is proportional to the frictional pressure gradient. If we assume that in annular-dispersed flow $2\tau_w/R$ is the main source of irreversibility, then a minimum in this curve corresponds to an equilibrium state. Such a minimum would provide an additional equation which could be used to move W_F from the input to the output side of the model. This appears to be an area requiring further study.

CONCLUSIONS

The proposed droplet interchange model for annular-dispersed flow successfully predicts several details of the flow not previously available. More specifically,

(1) By treating the droplets separately, instead of lumping them with the gas into a pseudo-fluid, we obtained two equations for the drag force on the droplet cloud. The first comes from momentum interchange between droplets and liquid film, the second from a summation, over all drop sizes, of the drag force exerted by an infinite turbulent gas stream on a single sphere. By equating these, we found the average velocity for each droplet size.

(2) When the drop velocity of (1) is equated to that contained in a critical Weber number, an expression for the maximum stable drop diameter results. Theoretical values of D_{max} are in good agreement with Wicks' [9] data.

(3) By assuming an exponential void profile through the film together with a 'universal velocity profile' near the wall matched to a linear profile near the interface, we calculated film thicknesses and velocities from a given wall shear stress. The latter is obtained, by iteration, from the known overall pressure gradient. Calculations for air–water flow in tubes of 3/8, 1/2 and 1·25 in. diameter show good agreement between measured and theoretical values of

mean film thickness
maximum-to-mean film thickness ratio
film crest velocity
liquid holdup.

(4) We defined the shear stress at the film-core interface, due solely to profile drag, by subtracting droplet drag and gas static head from the total pressure gradient and calculated interfacial friction factors from air–water data. The friction factors depended mainly on relative film thickness, regardless of tube diameter, gas Reynolds' number or liquid flow rate. They are comparable to those obtained by Wallis [4] for annular flow at negligible entrainment.

ACKNOWLEDGEMENTS

The work was carried out at McGill University and at the Chalk River Nuclear Laboratories. Atomic Energy of Canada Limited supported E. O. Moeck through an Educational Grant while the National Research Council of Canada provided an operating grant to the Computing Center at McGill University for the extensive use of their facilities.

REFERENCES

1. S. LEVY, Prediction of two-phase annular flow with liquid entrainment, *Int. J. Heat Mass Transfer* **9**, 171–188 (1966).
2. N. NISHIKAWA, K. SEKOGUCHI, M. NAKASATOMI, H. NISHI and A. KANEUZI, Liquid film flow phenomena in upwards two-phase annular flow, Paper No. 260, presented at the Jap. Soc. Mech. Eng. 1967 Semi-International Symp., Tokyo (1967).
3. L. BIASI, G. C. CLERICI, R. SALA and A. TOZZI, A theoretical approach to the analysis of an adiabatic two phase annular dispersed flow, *Energia Nucl., Milano* **15**, 394–405 (1968).
4. G. B. WALLIS, Annular two-phase flow—Part I: a simple theory, *J. Bas. Engng* **92**, 59–72 (1970).
5. G. B. WALLIS, Annular two-phase flow—Part II: Additional effects, *J. Bas. Engng* **92**, 73–82 (1970).
6. J. T. POGSON, J. H. ROBERTS and P. J. WAIBLER, An investigation of the liquid distribution in annular mist flow, *J. Heat Transfer* **92**, 651–658 (1970).
7. G. F. HEWITT, R. D. KING and P. C. LOVEGROVE, Liquid film and pressure drop studies, *Chem. Proc. Engng* **45**, 191–200 (1964).
8. SZE-FOO CHIEN and W. IBELE, Pressure drop and liquid film thickness of two-phase annular and annular-mist flows, *J. Heat Transfer* **86**, 89–96 (1964).
9. M. WICKS III, Liquid film structure and drop size distribution in two-phase flow, Ph.D. Thesis, University of Houston, Chem. Engng Dep. (1967).
10. D. E. WOODMANSEE and T. J. HANRATTY, Base film over which roll waves propagate, *A.I.Ch.E.Jl* **15**, 712–715 (1969).
11. N. ADORNI, P. ALIA, L. CRAVAROLO, A. HASSID and E. PEDROCCHI, An isokinetic sampling probe for phase and velocity distribution measurements in two-phase flow near the wall of the conduit, CISE Report R-89, Italy (1963).
12. G. H. ANDERSON and R. C. MANTZOURANIS, Two-phase (gas–liquid) flow phenomena—I. Pressure drop and holdup for two-phase flow in vertical tubes, *Chem. Engng Sci.* **12**, 109–126 (1960).
13. G. D. MCPHERSON and W. MURGATROYD, Film breakdown and dryout in two-phase annular flow, 3rd Int. Heat Transf. Conf., Vol. III, pp. 111–122, Chicago (1966).
14. D. B. SPALDING, A single formula for the 'Law of the Wall', *J. Appl. Mech.* **28**, 455–58 (1961).
15. A. KARNIS, H. L. GOLDSMITH and S. G. MASON, The flow of suspensions through tubes. V. Inertial effects, *Can. J. Chem. Engng* **44**, 181–193 (1966).
16. L. B. COUSINS and G. F. HEWITT, Liquid phase mass transfer in annular two-phase flow; droplet deposition and liquid entrainment, AERE-R5657, UKAEA, Harwell, England (1968).
17. J. O. HINZE, Fundamentals of the hydrodynamic mechanism of splitting in dispersion processes, *A.I.Ch.E. Jl* **1**, 289–295 (1955).
18. R. A. MUGELE and H. D. EVANS, Droplet size distribution in sprays, *Ind. Engng Chem.* **43**, 1317–1324 (1951).
19. L. E. GILL, G. F. HEWITT and P. M. C. LACEY, Sampling probe studies of the gas core in annular two-phase flow. Part II—Studies of the effect of phase flow rates on phase and velocity distribution, *Chem. Engng Sci.* **19**, 665–682 (1964).
20. L. B. COUSINS, W. H. DENTON and G. F. HEWITT, Liquid mass transfer in annular two-phase flow, Paper C4, Symposium on Two-Phase Flow, University of Exeter, **2**, C401–C430, England (1965).
21. W. D. HINKLE, A study of liquid mass transport in annular air–water flow, Sc.D. Thesis, Department of Nuclear Engineering, M.I.T. (1967).
22. L. E. GILL, G. F. HEWITT, J. W. HITCHON and P. M. C. LACEY, Sampling probe studies of the gas core in annular two-phase flow. Part I—The effect of length on phase and velocity distribution, *Chem. Engng Sci.* **18**, 525–535 (1963).
23. E. O. MOECK, Annular-dispersed two-phase flow and critical heat flux, Ph.D. Thesis, McGill University, Mechanical Engineering Department, Montreal (1970). Also AECL-3656, Chalk River, Canada.
24. G. F. HEWITT and B. NICHOLLS, Film thickness measurement in annular two-phase flow using a fluorescence spectrometer technique. Part II. Studies of the shape of disturbance waves, AERE-R 4506, UKAEA, Harwell, England (1969).
25. G. F. HEWITT and P. C. LOVEGROVE, Frequency and velocity measurements of disturbance waves in annular two-phase flow, AERE-R 4304, UKAEA, Harwell, England (1969).
26. R. M. NEDDERMAN and C. J. SHEARER, The motion and frequency of large disturbance waves in annular two-phase flow of air/water mixtures, *Chem. Engng Sci.* **18**, 661–670 (1963).
27. G. F. HEWITT, I. KING and P. C. LOVEGROVE, Holdup and pressure drop measurements in the two-phase annular flow of air–water mixtures, AERE-R 3764, UKAEA, Harwell, England (1961).
28. H. SCHLICHTING, *Boundary Layer Theory*, 4th Edn, p. 525. McGraw-Hill, New York (1962).
29. C. A. BANKSTON and D. M. MCELIGOT, Turbulent and laminar heat transfer to gases with varying properties in the entry region of circular ducts, *Int. J. Heat Mass Transfer* **13**, 319–344 (1970).

UN MODÈLE D'INTERCHANGE DE GOUTTES POUR UN ÉCOULEMENT BIPHASIQUE ANNULAIRE

Résumé—On présente une analyse d'écoulement annulaire dans laquelle l'écoulement est représenté par un film bidimensionnel et un coeur monodimensionnel de gaz porteur de gouttes. Le point essentiel de l'analyse est l'interchange de gouttes entre le coeur et le film et son transfert de quantité de mouvement associé. L'intensité du dépôt et de l'entraînement des gouttes commande la vitesse axiale associée à chaque dimension de goutte et permet le calcul du diamètre maximum d'une goutte stable en bon accord avec les mesures de Wicks.

Une distribution radiale exponentielle de vide et un profil de vitesse universel modifié à travers le film permettent le calcul des épaisseurs moyennes à la crête du film pour un débit du film donné. Ces calculs s'accordent bien avec les résultats de Harwell. Les facteurs de frottement à l'interface du uniquement à la traînée du profil sont aussi calculés et sont approximativement en bon accord avec les valeurs de Wallis pour des écoulements à entraînement négligeable.

EIN TRÖPFCHEN-AUSTAUSCH-MODELL FÜR ZWEIPHASEN-RINGSTRÖMUNG

Zusammenfassung—Untersucht wird eine Ringströmung, der als Modell eine zweidimensionale Film- und eine eindimensionale Strömung im Kern aus einem Tröpfchen-Gas-Gemisch zugrunde gelegt wird. Das Schwergewicht der Untersuchung liegt auf dem Tröpfchenaustausch zwischen Kern und Film und dem damit verbundenen Impulsaustausch. Die Intensität des Abscheidens und des Mitreissens von Tröpfchen bestimmt die axiale Geschwindigkeit der Tröpfchen aller Grössen und gestattet die Berechnung des Durchmessers des Tröpfchens maximaler Stabilität in guter Übereinstimmung mit den Messungen von Wicks.

Eine exponentielle, radiale Dampfverteilung zusammen mit einem modifizierten, universalen Geschwindigkeitsprofil über die Filmdicke erlaubt die Berechnung mittlerer und maximaler Filmdicken aus gegebenem Filmdurchfluss. Die Übereinstimmung mit Daten von Harwell ist gut, auch für die berechneten maximalen Geschwindigkeiten im Film. Faktoren der Reibung an den Berührungsflächen, die ausschliesslich auf Profilwiderstand zurückzuführen sind, werden ebenfalls berechnet. Sie stimmen annähernd überein mit Wallis' Werten für Strömungen, für die ein Mitreissen von Tröpfchen zu vernachlässigen ist.

МОДЕЛЬ КАПЕЛЬНОГО ОБМЕНА ДЛЯ КОЛЬЦЕВОГО-ДИСПЕРСНОГО ДВУХФАЗНОГО ТЕЧЕНИЯ

Аннотация—Представлен анализ кольцевого-дисперсного течения, когда оно моделируется как двумерная пленка и одномерный газовый сердечник со взвешенными капельками. Основное внимание сосредоточено на взаимном обмене капельками между сердечником и пленкой и связанным с этим переносом количества движения. Интенсивность оседания и уноса капелек влияет на аксиальную скорость частиц любого размера и позволяет рассчитать максимальный стабильный диаметр капли в хорошем соответствии с измерениями Вика.

Экспоненциальное радиальное распределение пустот вместе с модифицированным универсальным профилем скорости в плёнке позволяет рассчитать среднюю и максимальную толщину плёнки по данной скорости течения плёнки. Результаты хорошо согласуются с данными Харуэлла, как и рассчитанная максимальная скорость плёнки. Получены также коэффициенты межфазного трения, вызванного исключительно сопротивлением формы, которые находятся в приблизительном соответствии со значениями Уоллиса для течений с пренебрежимо малым уносом.